Bypass transition mechanism in a rough wall channel flow

Nisat Nowroz Anika* and Lyazid Djenidi†
Discipline of Mechanical Engineering, University of Newcastle, Callaghan NSW 2308, Australia

Sedat Tardu‡
LEGI, Université Grenoble Alpes Domaine Universitaire CS 40700, 38058, Grenoble Cedex 9, France

(Received 27 February 2018; published 21 August 2018)

The combined effect of wall pulsed jets and roughness in a laminar channel flow is investigated to determine whether or not turbulence can be triggered and maintained at low Reynolds numbers. The study is carried out through a direct numerical simulation based on the lattice Boltzmann method. The roughness, mounted on both walls of the channel, consists of transverse square bars spanning the whole width of the channel. Rectangular orifice(s) at the bottom wall act as pulsed jets. The jets are pulsed only once with the second jet activated at the end of the cycle of the first jet. Without activating the jets, the flow in the rough wall channel consists mainly in steady secondary motions in the canopies (spaces between bars) and a skimming two-dimensional laminar flow with some oscillations above the canopies. When the jets are activated, a localized three-dimensional turbulence develops and grows in the channel. Not only it is found that this localized turbulence bears strong similarity to that of a fully rough wall turbulent channel flow, but it appears to be in a "pseudo-" fully rough regime, as observed by the relatively negligible (averaged) viscous drag as compared to the form drag generated by the roughness elements. The physical mechanism which allows this to occur is discussed.

DOI: 10.1103/PhysRevFluids.3.084604

I. INTRODUCTION

The relatively rapid development of microtechnology allows extraordinary progress in miniaturization. In particular, microfluidics is a fast growing field because of its applications in many engineering disciplines such as chemical and biomedical engineering. Microfluidics covers several different areas of activities, e.g., miniaturization in microelectro-mechanical systems, DNA sequencing and drug delivery into blood, chemical reaction in microreactors, mixing and injection on laboratory-on-a-chip devices (see Refs. [1,2]), laboratory-on-a-stick itself (which is a recent phenomenon), and inkjet printing ([3]). However, one major hurdle yet to be well resolved and still under intense investigation is mixing between several streams of fluids in these microdevices. This is because the Reynolds number in microfluidic devices is too low to allow turbulence to be naturally generated. As a consequence, if left alone, the flow in microchannel remains laminar and mixing (through molecular diffusion) occurs at a very low rate. To increase mixing requires increasing the interfacial area between streams, which can be achieved by both active and passive methods. While there exists a wide range of mixing techniques within these two methods (see Ref. [4] for a relatively

*nisatnowroz.anika@uon.edu.au
†lyazid.djenidi@newcastle.edu.au
‡sedat.tardu@legi.grenoble-inp.fr

recent review of the two methods), we focus on a passive technique involving wall roughening (passive method) and an active method using pulsed jets at the wall (active method).

An important aspect of the mini-microchannel is their surface roughness, which is comparable to their cross-sectional dimensions because of manufacturing imperfections. Lammers *et al.* [5] performed a numerical simulation in a microchannel flow over a rough wall at Re $\simeq$ 1000 (Re $= U_b h/\nu$ where U_b is the bulk velocity, h the channel height, and ν the fluid kinematic viscosity). The roughness elements consisted of bars of rectangular cross section ($k = 17w$, where k and w are the height and width of the bar, respectively); the bar extended the wall width of the channel, and the spacing between two consecutive bars was $p = 96w$. The results show that turbulence can be self-maintained. However, turbulence was initiated at the start of the simulation by introducing random noise. Further, a periodic condition was imposed at the inlet and outlet on the computational domain as usual in turbulent channel direct numerical simulations. While this approach may be adequate from a numerical point of view, it is in fact not the actual representation of real microchannels, where there is no or negligible turbulence noise, and no periodic conditions are applied at the inlet and outlet of the channel. This raises an interesting question: Can turbulence develop and maintain itself in a low Reynolds number rough wall channel where the flow is initially laminar with no background turbulence and no periodic conditions are applied at the inlet and outlet of the computational domain? Hao *et al.* [6] performed particle image velocity measurements in a microchannel with three transverse square bars ($k = w$) mounted on one wall, with a spacing between the elements of about $p = 55w$. They report that the roughness elements lead to an earlier transition from laminar flow to turbulent flow as compared to a smooth microchannel flow; transition was observed to occur for Re ranging between 900 and 1100. They also show that the longitudinal velocity fluctuation begins to present a near-wall peak (on the rough wall side) at Re $\simeq$ 1000. Unfortunately, no data for the normal-to-the-wall and spanwise velocity fluctuations are presented. Note that the fluctuating velocity field in a vertical plane (x, y) at Re $\simeq$ 1800 shows the presence of coherent structures in the form of spanwise vortices. In the present study, we use square transverse bars to roughen channel walls. The bars are mounted on both walls of the channel with spacing $p = 8k$. The rationale for using $p = 8k$ stems from the results of Leonardi *et al.* [7]. These authors performed a direct numerical simulation (DNS) of a turbulent channel flow with transverse square bars mounted on one wall. They showed that when $p = 8k$, the drag coefficient is solely the form drag (the viscous drag is practically zero) and is maximum. This configuration thus corresponds to maximum turbulence generation and could be used to help trigger turbulence in a channel flow at low Reynolds number. This will be investigated in the present work.

Roughening a surface for generating turbulence in a laminar flow is a passive device. One active strategy that could be potentially effective to trigger turbulence in a a laminar channel would consist in applying a jet at the wall, such as synthetic jets [8]. Interestingly, Tardu *et al.* [9] undertook a direct numerical simulation in a laminar smooth channel flow at a Reynolds number of about 3000, based on the channel half-height and the centerline velocity. In their study, two pairs of counter-rotating vortices were injected in the flow in the form of stream functions represented by analytical expressions to investigate a bypass transition mechanism. They showed that the vortices interact near the wall in a manner which yields the compression (stretching) of the existing wall-normal vorticity induced by one of the pairs of the counter-rotating vortices, generating a new streamwise vorticity zone. This newly generated zone induces new coherent structures. These authors suggest that the key element in the process is the breakup of spanwise symmetry. The scenario leads to a self-maintaining autoregenerating coherent vortices. It appears that the mechanism is *a priori* Reynolds number independent as illustrated by Tardu and Nacereddine [10], who applied their bypass transition mechanism in a very low Reynolds number channel flow (Re $\simeq$ 10). They showed that it was plausible to generate "synthetic" turbulence in laminar flow at such a small Reynolds number if the system is suitably forced to prevent the damping effect of the viscosity. They further speculated that pulsed jets could be appropriate actuators for activating their bypass transition process. The bypass transition mechanism observed by Tardu *et al.* [9] may be exploited as a possible mixing strategy in low Reynolds number flows where turbulence is not sustainable (e.g., microfluidic systems). In the present work we investigate the use of wall pulsed jets to create a transition mechanism to trigger turbulence. The main reason to use this specific excitation process is to rapidly break up the spanwise symmetry as in Tardu *et al.* [9] and as will be clear later in this paper. We will indeed show that the rough channel is clearly subcritical unstable at $\mathrm{Re} \equiv 1000$. It will therefore transit to a fully developed regime when excited with noise, for example, as in Ref. [5] or using other kinds of local perturbations. This transition process will, however, require long time periods. We are not concerned with these aspects. The aim here is to see if one can induce local pseudo-fully developed turbulent spots in considerably short periods after only a few turnover times. The direct application of this process is enhancing mixing locally and on demand in a rough microchannel. So far studies on turbulent puffs generated by the wall jets, which indicated that local turbulence can be achieved temporarily in laminar pipe flows, were carried out at values of Reynolds numbers around the critical value ($\mathrm{Re} \simeq 2000$–3000) and never below it. It is then interesting to carry out study of wall jets in laminar pipe or channel flows to investigate whether or not localized turbulence can be achieved at values of Reynolds numbers lower than the critical value.

A DNS is carried out to perform an exploratory investigation of the use of passive and active methods, both separately and in combination, to generated turbulence-like flow in a laminar channel flow. The active method consists of using wall jets, and the passive method involves mounting roughness elements (square transverse bars) at the wall. It is the first time these two control methods are used simultaneously. The aim of the study is to ascertain the performance of each method individually and their combination with regard to possible turbulence generation in a laminar channel flow at a low Reynolds number. From a more fundamental point of view, and to our best knowledge, this is the first investigation dealing with bypass transition (BPT) process in a rough channel. The BPT mechanism is linked to the disturbance growth and breakdown on timescales shorter than regular Tollmien-Schlichting waves and their inherent secondary instability process in a subcritical wall bounded flow [11]. The finite-amplitude localized disturbances, which bypass the linear exponential growth, rapidly break down and form turbulent spots under subcritical instability. Turbulent spots have been numerically generated by using the initial localized disturbances in smooth plane Poiseuille and Couette flows [12,13]. Both the details of the bypass mechanism and the characteristics of local turbulence inside the spots were successfully elucidated in these investigations. There is a large literature on bypass transition over smooth walls, and the reader is referred to, for example, Gustavsson, Butler and Farrel, and Reddy and Henningson [14–16], who particularly investigated the nonmodal growth mechanism of initially localized perturbations. The setup of three-dimensionality leads to the achievement of finite amplitudes and of the nonlinear effects. The latter can, among other means, be generated by local surface irregularities such as roughness. We will show here, however, that this is not always the case, and that, curiously enough the particular roughness distribution used in the present subcritical flow results in a sustained two-dimensional (2D) turbulence. Triggering the three-dimensionality is plausible, however, by a simple methodology we will describe later in this paper.

II. NUMERICAL METHOD

A. Lattice Boltzmann method

A DNS is carried out via the lattice Boltzmann method (LBM, [17–19]). The LBM method is now well accepted as a viable numerical solver for fluid flows. Rather than solving the Navier-Stokes equations, the LBM solves the Boltzmann equation on a lattice.

The basic idea of the LBM is to construct a simplified kinetic model that incorporates the essential physics of microscopic average properties, which obey the desired (macroscopic) Navier-Stokes equations ([20]). With a sufficient amount of symmetry of the lattice, the LBM implicitly solves these latter equations with second-order accuracy. For the present calculations, each computational node consists of a three-dimensional (3D) lattice composed of 18 moving particles and a rest particle (lattice model $D3Q19$; for a developed account of LBM, see Refs. [21,22]). The method was successfully

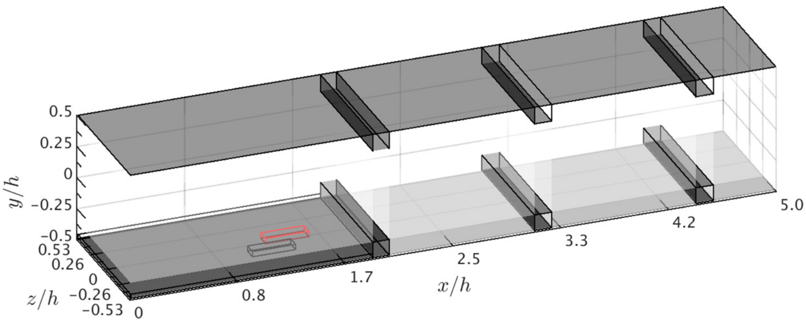

FIG. 1. Schematic of configuration of the channel (a short segment between the domain $0 \leqslant x/h \leqslant 5$). The jets are mounted only at the bottom wall (at $x/h = 1.09$) where two parallel plates are roughened by 2D square bars.

used for simulating both laminar [23] and turbulent flows [24]. Details of the method can be found in Ref. [24].

The motivation for the choice of LBM over the classical resolution of the Navier-Stokes equations has been presented in Ref. [24]. We briefly summarize the reasons here: (1) extreme ease of implementing solid surfaces of complex geometries, (2) no need for solving the Poisson equation for the pressure, and (3) ease of parallelizing the computations, which follows in part from the second reason and the fact that LBM is local in nature.

1. Computational domain and boundary conditions

The DNS are carried out in a Cartesian coordinate system. Figure 1 shows a schematic of the computational domain whose size is 17.7, h, and $1.07h$ in the x (axial), y (normal-to-the-wall), and z (spanwise) directions, respectively. The discretized mesh is $2100 \times 120 \times 128$, and the grid mesh increments in the three directions are $\Delta x = \Delta y = \Delta z$. The computations are carried out in the lattice units. Since the value of Reynolds number expressed in the lattice units ($\mathrm{Re}_{LB} = U_{LB}L_{LB}/\nu_{LB}$) is the same as the one expressed in the real physical dimensions ($\mathrm{Re} = UL/\nu$), one can easily retrieve the relationship between the lattice units and the real units. For example, setting Re also sets Re_{LB}. Thus, we have $\nu_{LB} = \mathrm{Re}/(U_{LB}L_{LB})$, which is related to the real viscosity as $\nu = (\Delta x^2/\Delta t)\nu_{LB}$. If, for example, we take $\Delta y = 1/h(= \Delta x)$, one can obtain Δt once ν is fixed.

The simulation is carried out at $\mathrm{Re} \simeq 1000$ for both smooth wall and rough wall channel flows. At the inlet, a parabolic velocity profile is applied while a convection condition is applied at the outlet (a zero gradient boundary condition was applied and a not significant difference was observed in the results). Periodic boundary conditions are applied in the spanwise direction at $z = 1$ and $z = n_z$. The velocity at the centerline of channel is denoted U_0. At the walls ($y = 1$ and $y = n_y$) a midgrid bounce-back scheme (no-slip at wall) is used which ensures a second-order accuracy [22]. It was verified that the simulation of a smooth laminar channel flow produced a velocity profile in a very good agreement with a Poiseuille distribution. Two jets are mounted at the bottom wall, which has a thickness of five mesh points (see Fig. 1). The jet orifices are of equal size with (41 mesh points along x and 12 mesh points along z). They are shifted in the z direction by a spacing $\delta_z = 16$ mesh points on both sides of the channel centerline. The center of the first orifice is located at $x = 151$, while the center of the second orifice is shifted downstream by a distance δ_x equal to 20 mesh points. At the jet inlet the following velocity profile is imposed:

$$u_{t,x,z} = u_0 \sin(\omega t)\sin(\pi x)\sin(\pi z), \tag{1}$$

where $0 < t < T$ (i.e., the jets are pulsed only once), $\omega = 2\pi/T$, with T an imposed time period, and the inlet velocity of jets is $u_0 = 16.6U_0$. Pulsing duration in dimensionless unit is $t^* = 0.033$. The input energy of jet is $E_j/U_0^2 = 2.2$ (in dimensionless units). The second pulsed jet is activated after the first pulsed jet has completed its blowing cycle. Our numerical experiments have shown that local puffs are also generated by a single jet, as expected. But a single jet (symmetric: mounted at the center of the bottom wall) has lesser ability to break down the spanwise asymmetry and to rapidly induce spanwise fluctuations. The paper deals with a feasibility concept for a rapid local transition in a rough subcritical channel. The optimum local-perturbation configuration requires further investigations that are out of our scope here. In the case of the rough wall channel flow, the roughness consists of square bars mounted transversally on both walls and spanning the entire width of the channel (see Fig. 1). The bar size or height is k (represented by 16 mesh points, i.e., $k/h = 0.133$), and the spacing between two consecutive bars is $p = 8 \times k$. As stated in the introduction, we selected this spacing $p = 8 \times k$ as it produced maximum drag [7]). The first bar is located at $x = 18k$ downstream of the second jet.

III. RESULTS

A. Flow visualization

A flow visualization is performed using the λ_2 method [25], which detects organized vortical structures. The method is based on the eigenvalues of the symmetric 3×3 tensor

$$M_{ij} = \Sigma_k (S_{ik} S_{kj} + D_{ik} D_{kj}) \tag{2}$$

with $k = 1, 2$, and 3 and

$$S_{ij} = \frac{1}{2}\left(\frac{\partial u_i}{\partial x_j} + \frac{\partial u_j}{\partial x_i}\right), \tag{3}$$

$$D_{ij} = \frac{1}{2}\left(\frac{\partial u_i}{\partial x_j} - \frac{\partial u_j}{\partial x_i}\right) \tag{4}$$

are the symmetric and antisymmetric components, respectively, of the velocity gradient tensor ∇u. The tensor M_{ij} has three real eigenvalues: λ_1, λ_2, and λ_3. Reference [25] argued that M_{ij} can be used to determine the existence of a local pressure minimum associated with vortical motion and showed that a vortex core can be identified as any continuous region where two of the eigenvalues of M_{ij} are negative. If the eigenvalues are sorted such that $\lambda_3 \leqslant \lambda_2 \leqslant \lambda_1$, then any region for which $\lambda_2 \leqslant 0$ corresponding to a vortex core. This method allows us to follow the development of any vortical structures in the flow.

Since, as expected, the flow visualization of the smooth wall channel flow confirmed that the flow was laminar when the wall jets were not actuated, we do not show the results of this flow visualization.

Figure 2 shows a snapshot taken shortly after the second jet had completed its blowing cycle, $t^* = 0.5$ (the asterisk denotes normalization by U_0 and $h/2$), for both the smooth and rough walls. At this stage, the two vortical structures (or turbulent puffs) generated by the jets are well separated and have not interacted yet. Notice though the complexity of the structures. It should be remembered that the second structure is generated after the first one. These structures are made up of “legs” and a “head” ([26]). The head is localized around the channel center region, while the tail is limited to the bottom wall region. Interestingly, we also observe a ringlike structure, likely to be a result of interaction among the turbulent puff parts, which deserves a dedicated investigation. However, since the focus of this work is not on the earlier development of these jet flow structures, we do not study further their characteristics nor their interaction.

One expects that the turbulent puffs, generated by the jets and subjected to the shearing associated with the mean velocity gradient, not only evolve with the flow but eventually interact between them and with the channel walls. In Fig. 3(a) we show a snapshot taken at $t^* = 3.5$ for rough wall after the jets were activated. The puffs have indeed evolved significantly into “trains of hairpins.” At this stage, we can see two trains of hairpins, each associated with the original puffs and attached on the

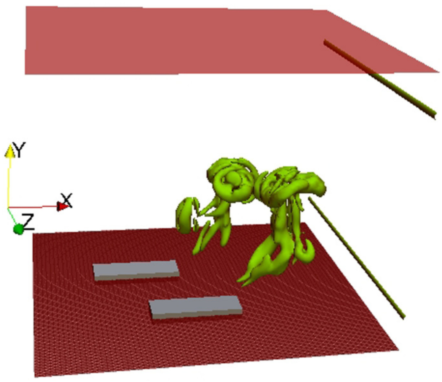

FIG. 2. Flow visualization-based λ_2 contour ($\frac{\lambda_2}{\lambda_{2,\max}} = -0.01$) at $t^* = 0.5$ on a rough wall, shortly after the jet(s) have complete their blowing cycle. The first orifice is placed behind the second orifice, which is shifted in the spanwise direction.

bottom wall. The remarkable feature to notice is the "bulky" nature of the vortical structure close to the upper wall. This structure results from a pressure effect. As the jets are activated, they create a pressure disturbance which propagates and reaches the top wall. The visualization showed that the phenomenon takes place almost instantly. However, a flow visualization comparison (not shown here) between smooth and rough walls reveals a noticeable difference between the smooth and rough cases as these puffs evolved. For example, in the case of rough wall pulsing, the hairpin legs are shorter and thinner than those observed on the smooth wall. The "bulky" head too is smaller on the rough wall than on the smooth wall. This difference is maintained as the structures evolve.

Figures 3(b) and 3(c) show snapshots taken at $t^* = 5.5$ and $t^* = 6.5$ in the case of rough wall. Of interest in this figure is the observation that the bulky head has now evolved into quasilongitudinal vortices. It should be said that there are more vortical structures on the rough wall than on smooth wall channel flow (not shown here), in conformity with the results of the Lammers *et al.* [5] and How *et al.* [6] results; i.e., the roughness is beneficial for enhancing or promoting turbulence. On the rough wall, we observe steady spanwise vortical structures residing at the wall between the roughness elements. These spanwise vortices [see Figs. 3(b) and 3(c)] reflect the secondary motion taking place as a result of the flow separation at the trailing edge of the bars.

To gain further insights into the time evolution of the vorticity on the rough wall with and without pulsing, we report in Figs. 4 and 5 isocountours of ω_z (the spanwise vorticity component) at two consecutive times in the region $2.5 \leqslant x/h \leqslant 7.5$ for both cases, i.e., inactive and activated pulsed jets. It is clear that the vortical motion caused by the roughness elements is disturbed by the passage of the structure generated by the pulsed jets. Notice the ejection of the fluid away from the wall (both bottom and top) and into the central region of the channel [Fig. 4(b)]. This suggests the following scenario taking place: as the vortical structure generated by the wall jets is convected downstream, it interacts with the secondary motion, pumping fluids out of the "cavities," while at the same time being stretched due to the shearing effect of the mean flow.

The secondary vortical motion taking place between the roughness elements is well visible in Fig. 6(a) which shows the streamlines (the velocities have been averaged over the span of the channel) in the region $2.5h \leqslant x \leqslant 5h$ for $t^* = 37.5$ (the reason why we selected this instant will become clearer later). When the jets are not activated, there is a distinct secondary vortical motion between two consecutive bars, over which the bulk of the flow skims without or little interaction with the secondary motion, as confirmed by the velocity fluctuation field shown in Fig. 6(c); there are virtually no fluctuations, and the flow remains 2D, i.e., the spanwise velocity component remains zero. The situation is quite different when the wall jets were actuated [Fig. 6(b)]. Since the disruption of the two-dimensionality of the flow is more important on the rough wall than on the smooth wall, we

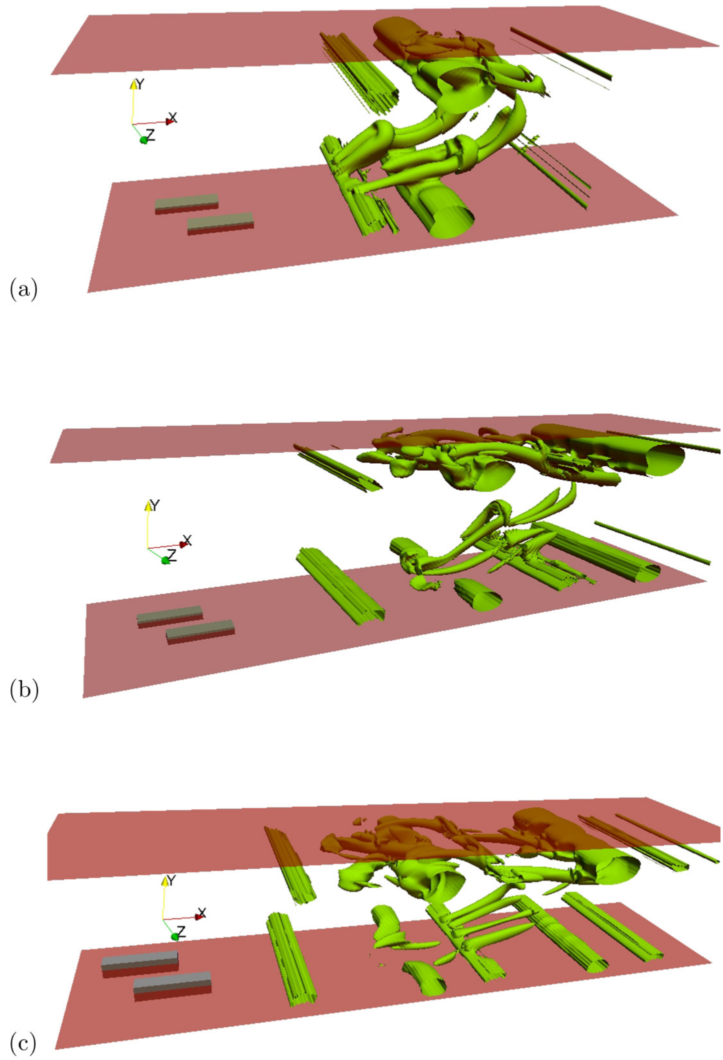

FIG. 3. Flow visualizations based on λ_2 contour ($\frac{\lambda_2}{\lambda_{2,\max}} = -0.01$) over the pulsating rough wall at (a) $t^* = 3.5$, (b) $t^* = 5.5$, (c) $t^* = 6.6$.

show only the rough wall case. Indeed, while the streamlines present similar features as in the case without pulsing, the velocity fluctuation field shown in Fig. 6(d) is dramatically different and reflects the three-dimensionality nature of the velocity field. Clearly, the activation of the pulsed jet leads to some turbulence generation. Yet at later time ($t^* = 65.5$) no difference is observed between the case with and without pulsed jets. This is because the turbulence generated by the pulsed jets has left the computational domain. This is well illustrated in Fig. 7, which shows isocontours of λ_2 at $t^* = 28, 32,$ and42, after the jets were activated. We can see clearly a "patch" of turbulence, mostly a group of hairpins moving with the fluid. Quite interestingly, at $t^* = 28$ and 32 most of the generated turbulence is located in the upper half of the channel, while at $t^* = 42$ it starts to occupy the whole channel, as it starts to leave the channel. This localized turbulence or turbulence "puff" is well seen in Fig. 8 as it has just started to leave the channel.

In summary, we found that the addition of roughness produces a secondary motion between the roughness, but the flow remained practically 2D. When the jets are activated, the disturbances

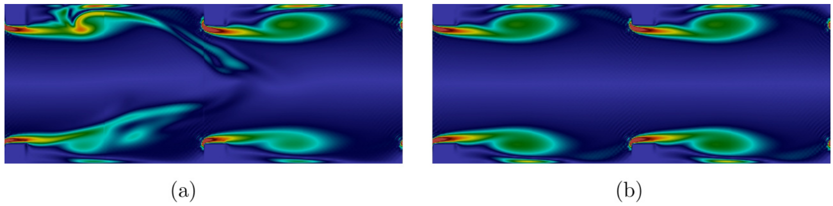

FIG. 4. Isocontours of ω_z at $t^* = 4.4$. (a) Rough wall without pulsing, (b) rough wall with pulsing; $2.5 \leqslant x/h \leqslant 5$.

generated by the jets lead to some "localized 3D turbulence" which is transported with the bulk flow. In the case of the smooth wall this "localized turbulence" is quickly dissipated by the action of the viscosity. In the case of the rough wall channel flow, the "localized turbulence" interacts with the secondary motion at the wall as it is convected with the bulk flow and, certainly due to this interaction, develops further and thus persists longer than on the smooth wall. Recalling that Leonardi *et al.* [7] showed that the (averaged) effect of viscosity near the wall is removed in the fully developed turbulent channel flow with a roughness similar to that used in the present study, it is possible that the "localized turbulence" is less affected by the viscosity and thus less dissipated than on a smooth wall and can, accordingly, survive for a longer time as it is transported. In the next section we try to quantify these observations through calculations of the mean velocity and Reynolds stress distributions.

B. Statistical analysis

As seen in the flow visualization, the structures generated by the pulsed jets are convected with the main flow and interact with the wall, generating further wall structures. Thus, from a statistical point of view the flow is not stationary or periodic, which presents a challenge for time averaging. Indeed, in this transitory flow the time-averaged values are dependent on the period over which the averaging is carried out. To ascertain an appropriate length of time over which a time average can be defined and which can lead to meaningful statistics, we computed the (normalized) total turbulent kinetic energy E within the computational domain as

$$\frac{E}{U_0^2} = \frac{1}{V}\frac{1}{2}\iiint (u^2 + v^2 + w^2)\, dx\, dy\, dz, \tag{5}$$

where the domain V of calculation is the entire channel. Figure 9 shows examples of the time variations of E for the rough wall with and without pulsing. Over the rough wall, without pulsing, E increases continuously until $t^* \simeq 8$ and then oscillates until $t^* \simeq 20$. Beyond this latter time, E presents a weak increase until $t^* \simeq 40$ and then drops slightly and reaches a plateau. When the jets are activated, the situation changes as seen in Fig. 9. First, notice (see inset of the figure) the two sharp peaks in E for $t^* \leqslant 0.1$ corresponding the energy input associated with the jets. After these two energy inputs, E decreases first until $t^* = 0.4$. Then it increases again and follows (while

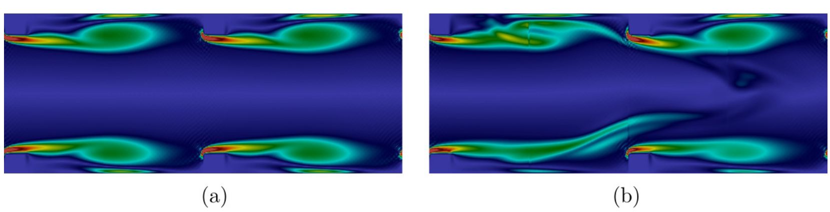

FIG. 5. Isocontours of ω_z at $t^* = 5.5$. (a) Rough wall without pulsing, (b) rough wall with pulsing; $2.5 \leqslant x/h \leqslant 5$.

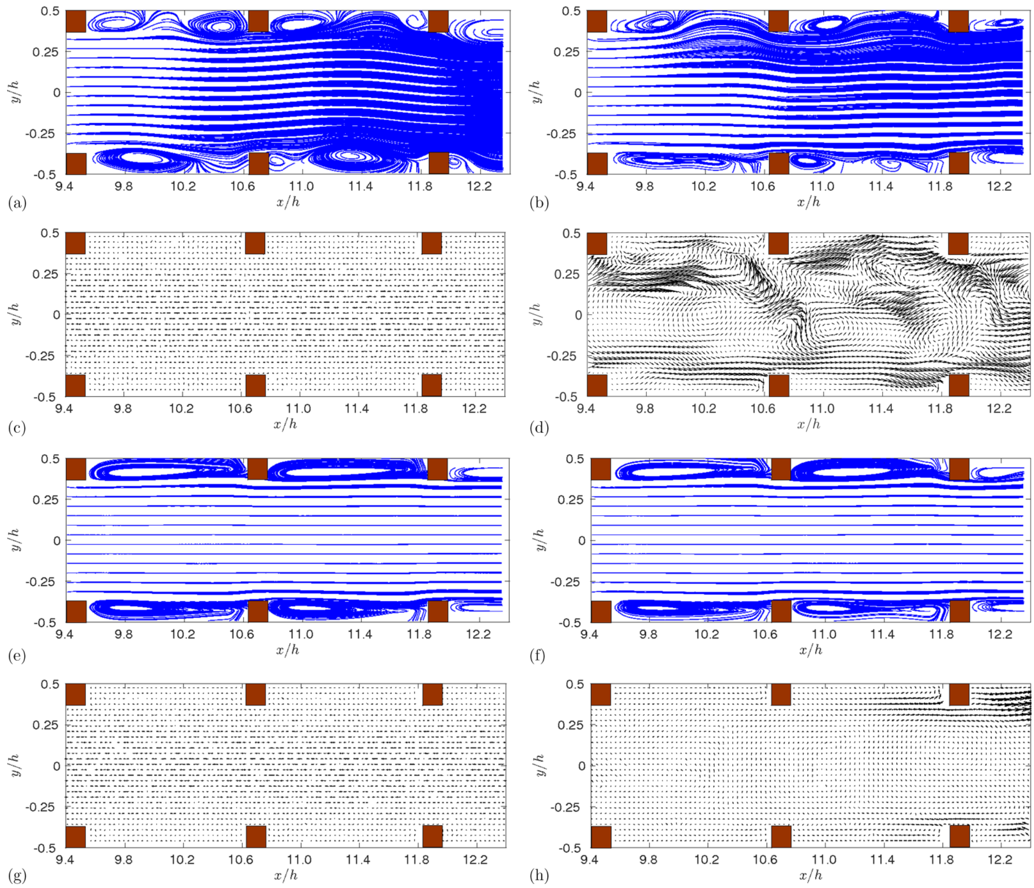

FIG. 6. Mean velocity streamlines in the (x, y) plane (averaged along z). $t^* = 37.5$: (a) rough wall, (b) rough wall with pulsing; $t^* = 65.5$: (e) rough wall, (f) rough wall with pulsing. Vector fields of the velocity fluctuations in the (x, y) plane (averaged along z). $t* = 37.5$: (c) rough wall, (d) rough wall with pulsing; $t^* = 65.5$: (g) rough wall, (h) rough wall with pulsing.

being slightly higher than) the energy without pulsing until $t^* = 12$. As t^* increases, E increases at a much greater rate than that without pulsing, reaches a maximum at $t^* \simeq 38$, and drops to the same plateau as that without pulsing. The message of Fig. 9 is clear: the roughness does promote some turbulent energy. The bypass transition mechanism provoked by the roughness itself reaches a sustained steady state at $t^* = 40$. We will show that the latter corresponds to the setup of a 2D turbulence field wherein there is lack of spanwise velocity fluctuations. When the jets are activated, the generated local vortical structure breaks the spanwise symmetry near the peak of the transient in Fig. 9, and 3D localized turbulence can grow as it moves with the mean flow. As can be inferred from the flow visualization, the vortical structures generated by the pulsed jets eventually will leave the computational domain. Figure 9 indicates that this occurs at $t^* > 50$ wherein the 2D turbulent field is recovered.

A comment is warranted on the physical mechanism by which the pulsed jets can lead to a significant localized turbulence on the rough wall and not on the smooth wall. We already said that the global viscous drag on a fully rough wall is negligible in comparison to the form drag generated by the roughness elements. Table I shows the coefficients of the viscous drag and form drag and their summation. The values represent double spatial (along the z direction) and time ($38 \leqslant t^* \leqslant 42$) averaged quantities. The viscous drag is calculated by integrating $\mu(du/dy)$ at the wall over $x = p$

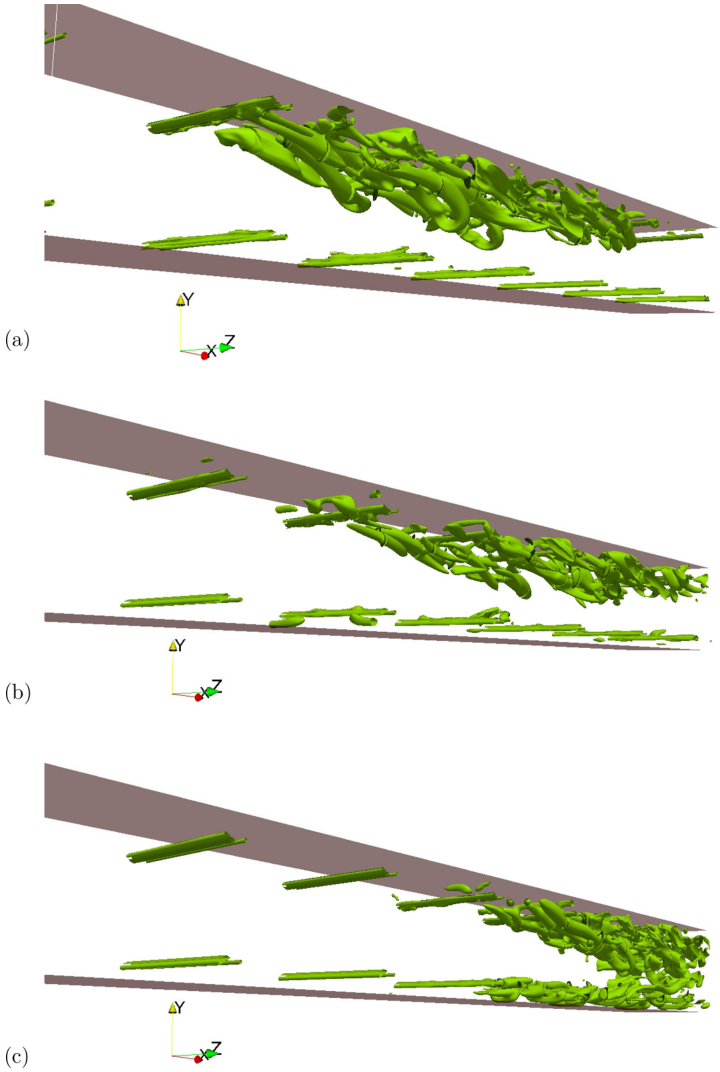

FIG. 7. λ_2 contour ($\frac{\lambda_2}{\lambda_{2,\max}} = -0.01$) at (a) $t^* = 28.0$, (b) $t^* = 32$, and (c) $t^* = 42$. The region shown corresponds to $7.5 \leqslant x/h \leqslant 12.5$.

in the domain between $11.4 \leqslant x/h \leqslant 12.5$ represented in Fig. 8, while the form drag is computed from the pressure distribution around a bar.

Although the turbulence is not fully developed, the viscous drag is, quite remarkably, practically negligible. We have also evaluated the total drag using a momentum balance and found it is equal to that of the form drag, confirming that the viscous drag is negligible. These results indicate that the near-wall viscous effect is on average negligible (as expected from Fig. 6, most of the viscous drag is generated at the top of the roughness elements; between the roughness element the viscous drag is very small and negative). Accordingly, the turbulent structure generated by the jets interacts with the roughness in a "viscous-free environment" with a low dissipative effect allowing turbulent energy to be produced and grow.

We can now use Fig. 9 to fix the length of time for time averaging for the rough wall. One would be inclined to carried out time averaging for $70 \leqslant t^* \leqslant 100$, when the flow is in a steady-state regime.

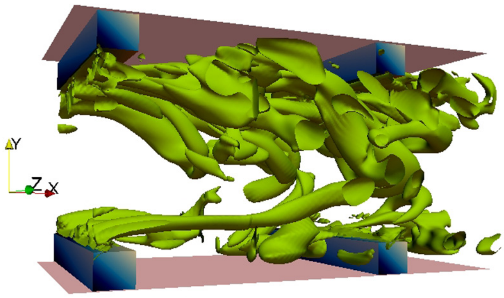

FIG. 8. Visualization of the localized turbulence at $t^* = 42$ based on λ_2 criteria.

However, this would fail to capture the statistics induced by the localized 3D turbulence, when the jets are activated. Indeed, the turbulent puffs leave the computational domain at $t* > 60$. For this reason, it is preferable to carry out a spatial averaging limited (hereafter called limited spatial average) in x and z at a single time $t^* = 42$ around the localized turbulence shown in Fig. 8. This is expected to provide a more accurate representation of the localized turbulence characteristics resulting from the activation of the wall jets. Thus, all the statistics we will present hereafter in the rough channel with and without pulsating jets are obtained through the limited spatial average procedure.

C. Mean velocity

Figure 10 shows the profiles of the mean velocity $U^+ = U/u_\tau$ as a function of $y^+ = yu_\tau/\nu$ (u_τ is the friction velocity, and superscript $''+''$ denotes normalization with respect to u_τ) for the smooth and rough walls with and without jets and averaged as described above. For completeness, we also report in the inset of the figure the profiles corresponding to the time- and spatial-averaged profiles over the entire channel for the steady-state regime ($70 \leqslant t^* \leqslant 100$); u_τ is calculated via the pressure gradient:

$$u_\tau = \sqrt{\frac{h(dp/dx)}{\rho}}, \tag{6}$$

where ρ is the density of fluid, and p the pressure For the limited spatial average, u_τ is calculated via a momentum balance over a control volume enclosing the localized turbulence shown in Fig. 8. A semilog representation is used to better reveal the near-wall region; note that only the lower half-channel is considered. Further, since the velocity profile for the smooth wall without a jet is a Poiseuille distribution, we do not show it in the figure. Data of fully developed turbulent flows in rough channels at low Reynolds numbers are rare in the literature. The Karman number based on the half width of the channel $\mathrm{Re}_\tau = \frac{h\overline{u_\tau}}{2\nu}$ varies, for example, from 400 (DNS) to 600 (experiments) in Krogstadt's investigation [27] (not shown here), while the Re_τ is only 100 in the present study. The letter is closer, however, to $\mathrm{Re}_\tau = 60$ of Lammers *et al.* [5], and this is the reason why we use these latter data to compare with our results. As indicated in the introduction, Lammers *et al.* carried out a DNS based on the LBM of a fully developed turbulent rough channel and used (thin) obstruction

TABLE I. Drag coefficient.

Variable	Values
$C_{f,\mathrm{visc}}$	5.769×10^{-5}
$C_{f,\mathrm{form}}$	1.69×10^{-2}
$C_{f,\mathrm{visc}} + C_{f,\mathrm{form}}$	0.0169

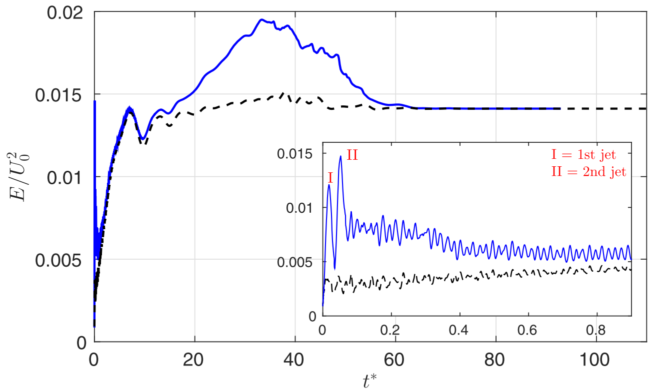

FIG. 9. Time variation of the averaged kinetic energy E for the rough wall with two pulsing (——), without pulsing (- - - - -). Inset: early stage of during and after jets in between $0 \leqslant t^* \leqslant 0.9$.

elements spanning the width of the channel, with $k/h = 0.133$, $w/k = 0.058$, and $p = 5.6k$. In Fig. 10 we report the mean velocity profile at the midpoint between two roughness elements, provided by these authors.

Let us first consider the steady-state regime ($70 \leqslant t^* \leqslant 100$). When the jets were activated in the smooth wall case, the profile does not differ significantly from that of the Poiseuille distribution (not shown here). On the rough wall with and without pulsing, U^+ presents the same distribution at that for the smooth wall but is shifted downward, reflecting the increase of u_τ by the rough wall. As expected, the profiles on the rough wall with and without the jets are similar since the localized turbulence generated by the jets left the channel before this time interval.

When the jets are activated, the velocity profile is dramatically altered. Note that since the flow is not symmetric with respect to the centerline, as hinted by the flow visualization, at this time at least (see Fig. 8), we report both the lower and upper parts of velocity distribution. First, there is a strong downward shift, which indicates, as expected, that the value of the limited spatial averaged u_τ is

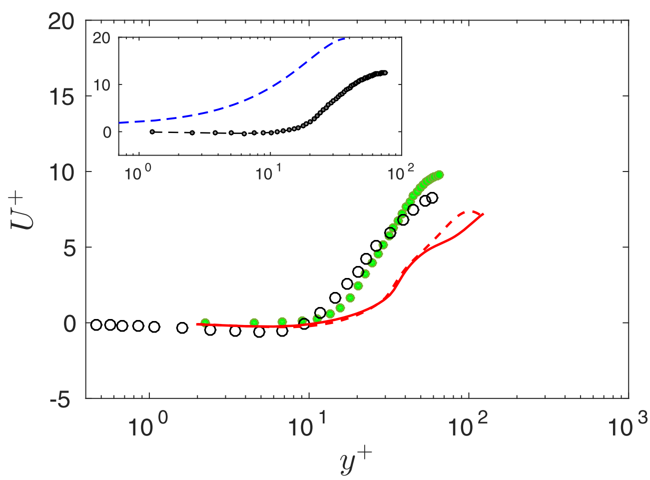

FIG. 10. Normalized mean velocity profiles for the limited spatial averaging at $t^* = 42$ for a rough wall: without pulsing (●) and two pulsing (——: upper half), (- - - - -: lower half). DNS of a fully developed turbulent rough channel flow [5] (open symbols). Inset: Double (time and space) averaged; - - - - -: smooth wall with jets; -●-: smooth wall without jets.

larger than the time- and space-averaged value. Second, the profiles tend to show the emergence of a log region (more evident for the upper part velocity profile than the lower part) and suggest that, over a limited portion of the channel, the localized turbulence presents features commonly observed in a fully developed turbulent channel (at least on a rough wall). Notice that the lower part velocity profile is quite similar to that of Ref. [5], but shifted downward. The comparison between the profile of Ref. [5] and the present rough wall ones with and without pulsing is interesting, in that it helps us to answer the question raised in the introduction regarding the generation and sustainability of turbulence in a low Reynolds number rough channel where the flow is initially laminar with no background turbulence and no periodic condition in the streamwise direction. Reference [5] used periodic conditions at the inlet and outlet of the computational domain. Further Ref. [5] stated that they are started their simulation with an initial velocity field but did not show it. However, their Fig. 6 clearly indicates that a background noise was used. The use of random noise combined with the periodic condition in the streamwise and spanwise directions provides ideal conditions to precipitate turbulence. Indeed, the background noise can trigger some instability in the flow, which is recycled into the flow via the periodic conditions. Clearly, this led to a fully developed turbulent channel flow. The present results show that, if these ideal flow conditions are not used, then it is likely that the flow would not become turbulent, unless the channel is relatively quite long to allow any instability to grow and eventually leads to turbulence. As indicated before, and as will be seen in detail below, the flow structure over the rough wall without jets activation is a 2D turbulence with $u'_3 \equiv 0$. The latter are setup by jets activation that increases the local wall shear stress beyond its fully developed equilibrium value. Recall, however, that the process is particularly rapid, and it cannot be expected to reach the fully developed regime only after a few dozen large eddy turnover times. Interestingly, though, the downward shift of the present profiles with respect to Ref. [5] is due to a strong roughness effect.

D. Reynolds stresses

The velocity distributions shown in Fig. 10 clearly indicate that the results obtained from time and spatial averaging across the entire channel are not representative of the localized nature of the turbulence generated in the channel by the pulsed jets. Further, as seen from Fig. 9 and the flow visualization, the localized turbulence begins to leave the computational domain at $t^* \simeq 37$–40. Thus, we focus our attention on times for which the localized turbulence can be relatively well identified. In the subsequent analysis, the double spatial averaging in x and z is carried out for $10.6 \leqslant x/h \leqslant 17.5$ only and over the entire spanwise length of the channel.

We report in Fig. 11 the distributions of the velocity rms u'_i and the rough wall with and without pulsing (the overbar represents averaging over x, z, and t, and $i = 1$, 2, and 3 represents the x, y, and z directions, respectively) at $t^* = 42$, which corresponds to the snapshot shown in Fig. 7(c). The Reynolds number of the smooth channel is 3/4 times smaller than the critical Orszag number ([28]) below which any perturbation disappears in a smooth channel. Thus, the wall activation induced by pulsed jets in the smooth wall case does not lead to any sustained local turbulence, and, consequently, we do not show the corresponding results here.

On the rough wall and when the jets are not activated [Fig. 11(a)], one can observe that the longitudinal, u'_1, and normal-to-the-wall, u'_2, components are not negligible, but the spanwise component, u'_3, is zero, confirming the 2D nature of the localized turbulence generated by the roughness elements. Of interest is that not only is u_1 zero in the central part of the channel, but u'_2 is quite important in that region; in fact, u'_2 is practically constant across the channel. This was at first puzzling, but it was then realized that the source of the large values of u'_2 in the central part of the channel was a large-scale oscillation occurring in the flow, which can be seen in Fig. 6(a) for $x/h \geqslant 10$; this explains the almost constant value of u'_2 across the channel.

These results alone are interesting and deserve some comments. The 2D perturbed flow field is clearly sustained. All three components of the fluctuating vorticity field are nonzero and are reduced to $\omega_x = -\frac{\partial v}{\partial z}$ in the streamwise, $\omega_y = -\frac{\partial u}{\partial z}$ in the wall-normal, and $\omega_z = \frac{\partial v}{\partial x} - \frac{\partial u}{\partial y}$ in the spanwise

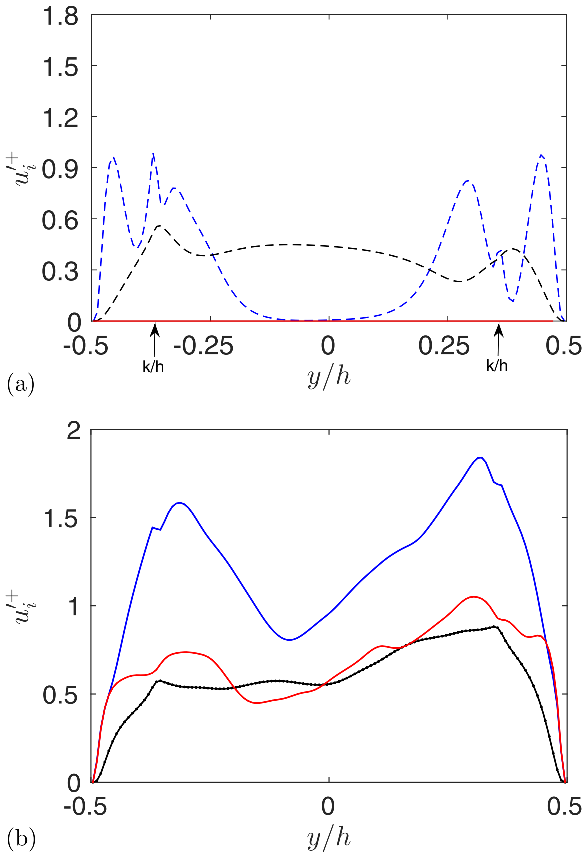

FIG. 11. Distributions of the velocity rms $u_i'^+$ at $t^* = 42$ on the rough wall: (a) without jet (u_1': - - - -; u_2': - - - -; u_3': ——); (b) with two jets (u_1': ——, u_2': ——, u_3': ——).

directions since $w \equiv 0$. Yet the main production term $-\frac{\partial w}{\partial x}\frac{\partial U}{\partial y}$ in the streamwise vorticity transport equation

$$\frac{D\omega_x}{Dt} = \left(\frac{\partial w}{\partial y} - \frac{\partial v}{\partial z}\right)\frac{\partial u}{\partial x} - \frac{\partial w}{\partial x}\frac{\partial (U+u)}{\partial y} + \frac{\partial v}{\partial x}\frac{\partial u}{\partial z} + \nu\frac{\partial^2}{\partial x_l \partial x_l}\omega_x \tag{7}$$

resulting from the tilting of the wall normal vorticity is now missing. The streamwise vorticity layers are therefore relatively weak. The setup of w and more importantly the regeneration of $-\frac{\partial w}{\partial x}$ are necessary to generate ω_x layers that after roll-up lead to strong energetic quasisteamwise vortices. When the jets are activated on the rough wall [Fig. 11(b)], the distributions u_i' present similar characteristics to those observed in a fully developed turbulent channel flow. Notice though the nonsymmetric feature of the distributions associated with the asymmetrical nature of the localized turbulence as shown in the flow visualizations.

The difference between the cases with and without pulsing on the rough wall warrants a comment. When the jets are activated, the resulting jet flow structure breaks up the symmetry in the spanwise direction, thus generating some spanwise velocity fluctuations and local gradients $\frac{\partial w}{\partial z}$, which, in turn, through the pressure-velocity gradient correlation $\Pi_w = p\frac{\partial w}{\partial z}$ [29], helps transfer energy to w, resulting in its growth.

In order to assess the roughness regime (e.g., transient or fully rough) of the localized turbulence, we compare in Fig. 12 the distributions shown in Fig. 11(b) (only the lower part of the distributions)

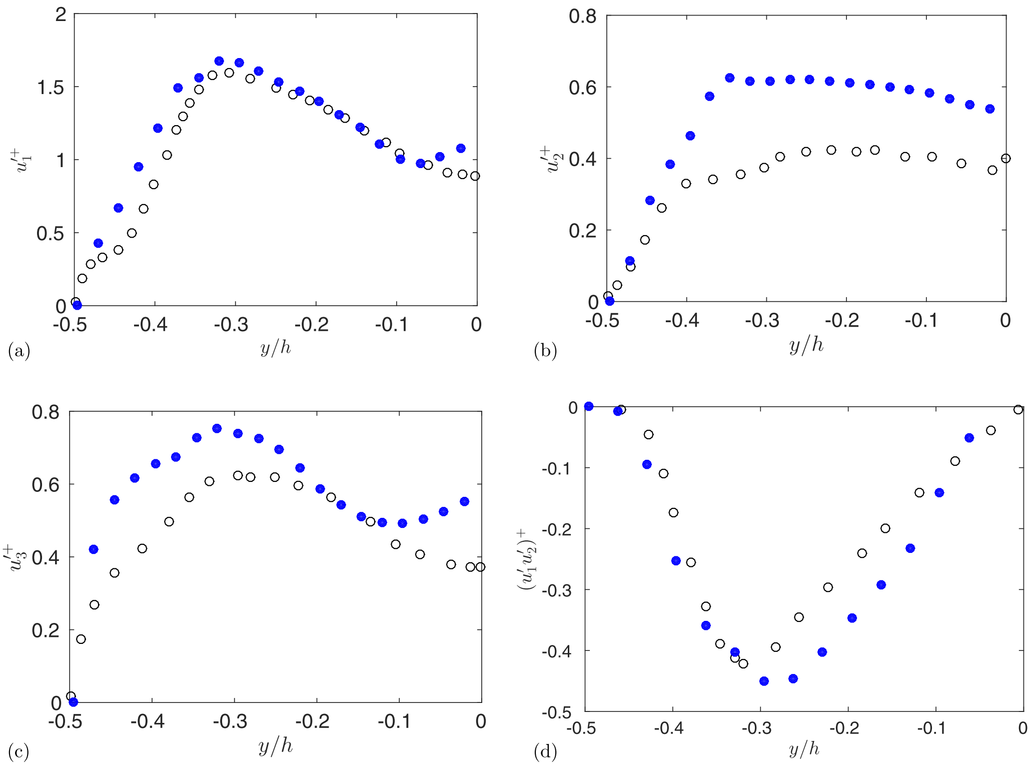

FIG. 12. Nondimensionalized root mean square (rms) velocity fluctuations (a, b, c) and Reynolds shear stress (d) distributions on a rough wall with two jets at $t^* = 42$ (closed symbols) compared to the DNS at a similar Reynolds number of a fully developed rough channel [5] (open symbols) (see the text for details).

with the results of the low Reynolds number DNS rough wall data of Ref. [5]. Since the results of Ref. [5] are time averaged only, the Reynolds stress profiles, close to the wall, vary with the streamwise position between the roughness elements; for a comparison with our results we selected the distributions obtained at a midpoint between two roughness elements (e.g., Fig. 8 at $x_1^+ = 53$ in Ref. [5]). Accordingly, perfect quantitative correspondence between the convected turbulent puff induced velocity fluctuations intensities and those of Ref. [5] cannot be expected, and the comparison can be only on a qualitative basis. Quite remarkably, though, there is a good agreement between the

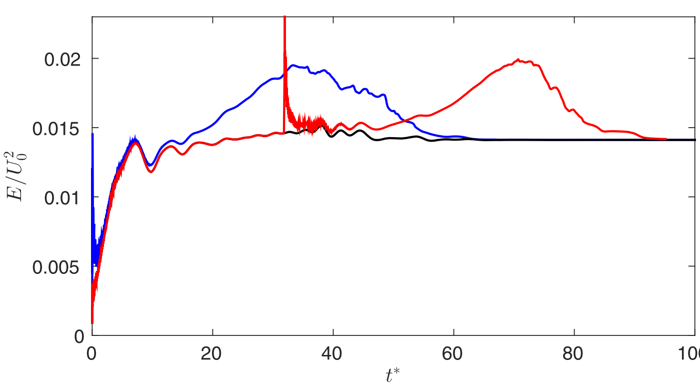

FIG. 13. Time variation of the averaged kinetic energy E for a rough wall with jets at $t^* = 30$ (pulsating at $t^* = 0$: ——; pulsating at $t^* = 30$: ——; without jets: ——).

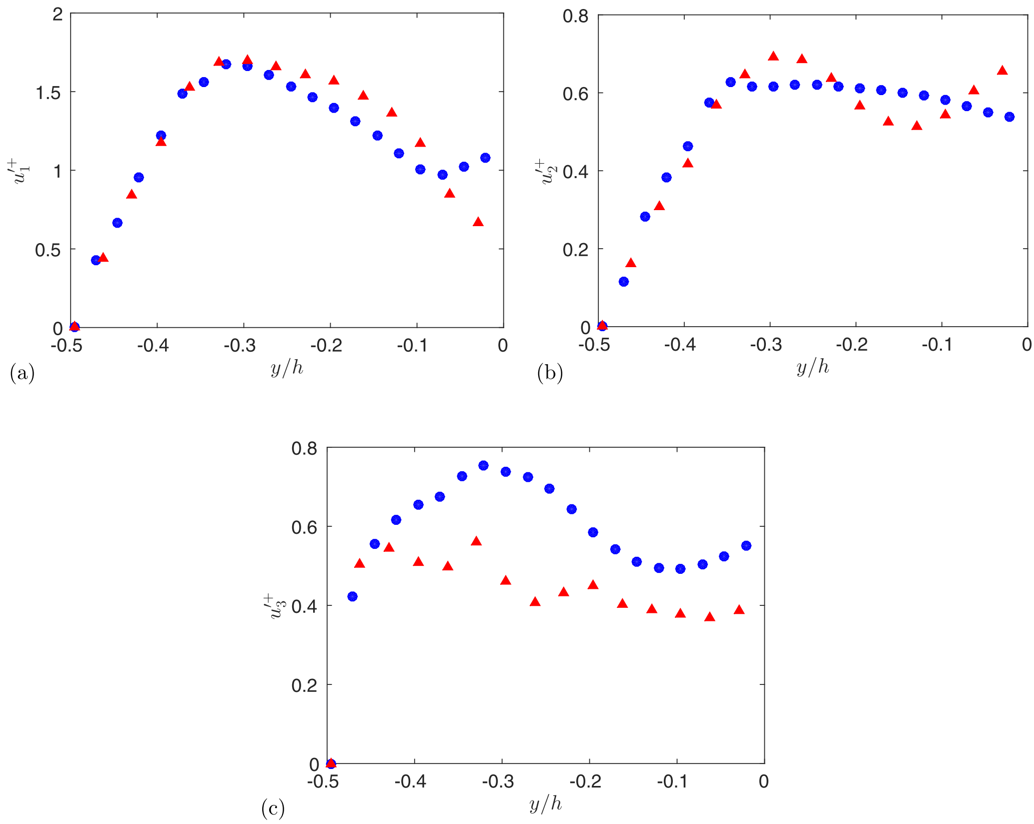

FIG. 14. Distributions of nondimensionalized rms velocity fluctuations on a rough wall with two jets activated at $t^* = 0$ ($t^* = 42$, closed circles) and at $t^* = 30$ ($t^* = 76$, closed triangles).

distributions of the streamwise velocity rms $u_1'^+$ and Reynolds shear stress $(u_1'u_2')^+$ induced by the tracked turbulent puff and those of fully rough ones [5]. Note that the present distributions of $u_2'^+$ and $u_3'^+$ show larger differences from their DNS counterparts than $u_1'^+$ and $(u_1'u_2')^+$. This indicates that the intercomponent transfer mechanism between the turbulent shear stress components $\overline{u_i'u_i'}$ has not had enough time to be established yet at $t^* = 42$. Despite these differences, these results, taken as a whole, would suggest that the localized turbulence is in a "pseudo-" fully rough regime.

The main objective addressed in this work was to investigate the combined effects of passive (roughness) and active local perturbations on the bypass transition through identical initial conditions. Consequently the pulsed jets were activated at $t^* = 0$. The immediate question that arises is how does the system behave when the jets are activated after the pseudo-2D turbulence over the rough wall is achieved, in the present case at typically $t^* \geqslant 30$? Figure 13 compares the time variation of the averaged kinetic energy between the case where the jets activated at $t^* = 0$ (hereafter labeled case A) and at $t^* = 30$ (case B). It is seen that the maximum of E/U_0^2 occurs at $t^* = 70$ in case B resulting in a shift $\Delta t^* = 40$ with respect to the activation time. That compares well with $\Delta t^* = 35$ of the case A. The magnitudes of the maximum of E/U_0^2 during the transients are also closely similar. This is curious and not *a priori* expected since the system is nonlinear. The time durations of the transients also compare well in Fig. 13, but the energy distributions versus time are not completely identical, the decrease of E following its maximum being sharper in case B (Fig. 13).

The limited spatial averaging procedure is applied at $t^* = 76$ in case B for comparison with the limited spatial averaging of case A at $t^* = 42$. The value $t^* = 76$ corresponds to the time at which the energy E/U_0^2 in B is identical to $t^* = 42$ for case A. This choice may be questionable since the

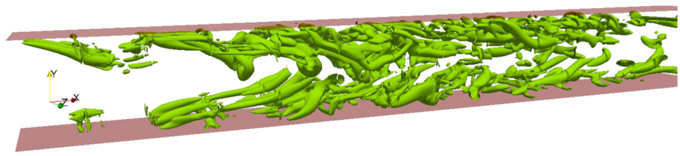

(a)

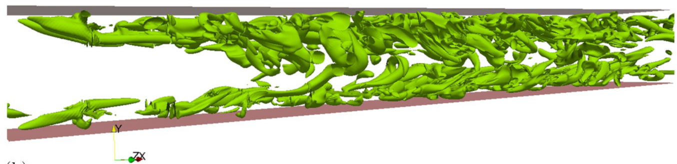

(b)

FIG. 15. Flow visualization based λ_2 contour ($\frac{\lambda_2}{\lambda_{2,\max}} = -0.01$) at $t^* = 42$ on the rough wall: (a) one jet, (b) two jets. The region shown corresponds to $8.1 \leqslant x/h \leqslant 17.5$; the section $x/h = 17.5$ is the channel outlet.

time-space development of the 3D puff is different in both cases. Thus, E/U_0^2 may be revealed not to be the adequate similarity variable, but the comparison is only of a qualitative nature here. While the mean velocity U^+ changes only marginally, the flow is found to be more symmetrical with respect to the channel centerline in case B than in case A (not shown). We compare in Fig. 14 the velocity rms profiles for both cases. It is of course out of question to expect a perfect quantitative collapse. Yet it is seen that the $u_i'^+$ profiles compare qualitatively well. In conclusion, the activation of the jets once the 2D turbulence is achieved leads to the same results as when they are activated before. This illustrates clearly the ability of wall pulsed jets to precipitate the 3D turbulence over the rough wall through a bypass transition mechanics.

As briefly discussed earlier, a single jet also induces a local puff and 3D perturbations. Figures 15(a) and 15(b) show the coherent structures induced by one and two jets, respectively, for qualitative comparison purposes. Double pulsing leads clearly to a significantly denser structure population near both the upper and lower walls. Figure 16 compares the rms of the streamwise and spanwise velocity fluctuations profiles at $t^* = 42$, obtained through the same averaging procedure as before, in

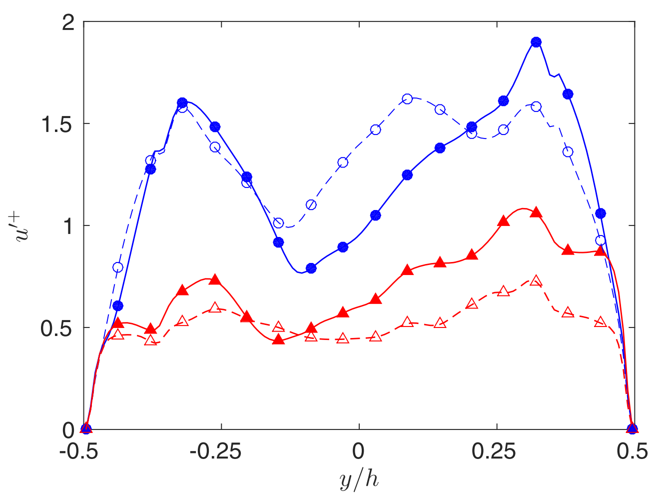

FIG. 16. Distributions of the velocity rms $u_i'^+$: one jet (u'^+: - ○-, w'^+: -△-), two jets (u'^+: -●-, w'^+: - ▲-) at $t* = 42$.

both cases. The wall normal velocity $u_2'^+$ profiles were found to be more or less similar, and they are not shown for the sake of clarity. Note, first, that the pseudoturbulent spanwise velocity fluctuations intensity $u_3'^2$ is at least twice smaller with one jet than two jets. We attribute this difference to a higher capacity of the two jets to break up the spanwise symmetry, but a systematic parametric study is needed to confirm this hypothesis. Note also in Fig. 16 that this is a significant departure in the spanwise velocity rms $u_1'^+$ profile induced by one jet compared to two jets in the outer layer. It is plausible that the subcritical flow over the rough wall evolves to a similar regime under one single pulsed jet but after a significantly longer time.

IV. CONCLUSION

A DNS using the lattice Boltzmann method is carried out in a laminar channel flow at a subcritical Reynolds number (Re $=$ 1000 based on the height of the channel). Both rough walls with single- and double-wall pulsed jets are considered. The roughness (at both walls of the channel) consists of transverse square bars spanning the whole width of the channel. The distance between two consecutive bars is eight times of a bar side. Two rectangular orifices at the bottom wall act as jets; the jets are pulsed only once with the second activated at the end of the cycle of the first jet.

The activation of the jets changed dramatically the flow over the rough wall. When the jets are not activated, secondary motion develops within the canopies (space between bars), and the bulk flow skims over it without much interaction. The flow remains 2D and quasilaminar. When the jets are activated, the resulting 3D jet flow structure interacts with the secondary motion in the canopies and breaks the two-dimensionality of the flow. After some time, a localized 3D turbulence develops and grows as it is transported with the bulk flow. It is observed that this localized turbulence shares similar features (at least in terms of the mean velocity and Reynolds stress distributions) with those of a fully rough wall turbulent channel flow. In particular, it appears that the localized turbulence is in a "pseudo-" fully rough regime, as observed by the relatively negligible (averaged) viscous drag as compared to the form drag generated by the roughness elements. This could explain why the turbulence can grow: the 3D instability created by the jets can evolve in an environment where the dissipative effect associated with the viscosity is negligible. From a practical point of view, the present study indicates clearly that the combination of wall pulsed jets and roughness can be effective in generating and maintaining turbulence in a low Reynolds number channel flow. Tardu [30] has shown that self-developing and self-generating turbulent-like quasistreamwise vortices can be triggered at Reynolds numbers as small as Re $=$ 10, in a smooth channel, when the laminar base flow is suitably and continuously forced. Spots that are curiously similar to the wall turbulent puffs are obtained this way. In parallel, it is asked here whether proceeding in a similar way over a rough wall can help maintain turbulence not only over a longer time but also over a longer channel. The subsidiary question is the minimum value of the Reynolds number at which feasible continuous wall actuation would still lead to the persistence of local pseudodeveloped turbulent puffs.

---

[1] C.-C. Chang and R.-J. Yang, Electrokinetic mixing in microfluidic systems, Microfluid. Nanofluid. **3**, 501 (2007).

[2] T. Vilkner, D. Janasek, and A. Manz, Micro total analysis systems. Recent developments, Anal. Chem. **76**, 3373 (2004).

[3] K. Maejima, S. Tomikawa, K. Suzuki, and D. Citterio, Inkjet printing: An integrated and green chemical approach to microfluidic paper-based analytical devices, RSC Adv. **3**, 9258 (2013).

[4] C.-Y. Lee, C.-L. Chang, Y.-N. Wang, and L.-M. Fu, Microfluidic mixing: A review, Int. J. Mol. Sci. **12**, 3263 (2011).

[5] P. Lammers, J. Jovanović, and A. Delgado, Persistence of turbulent flow in microchannels at very low Reynolds numbers, Microfluid. Nanofluid. **11**, 129 (2011).
[6] P.-F. Hao, Z.-H. Yao, F. He, and K.-Q. Zhu, Experimental investigation of water flow in smooth and rough silicon microchannels, J. Micromech. Microeng. **16**, 1397 (2006).
[7] S. Leonardi, P. Orlandi, R. J. Smalley, L. Djenidi, and R. A. Antonia, Direct numerical simulations of turbulent channel flow with transverse square bars on one wall, J. Fluid Mech. **491**, 229 (2003).
[8] A. Glezer and M. Amitay, Synthetic jets, Annu. Rev. Fluid Mech. **34**, 503 (2002).
[9] S. Tardu, R. Nacereddine, and O. Doche, An interactive bypass transition mechanism in wall-bounded flows, J. Fluid Mech. **615**, 345 (2008).
[10] S. Tardu and R. Nacereddine, A new active micro-mixing strategy, Heat Transfer Eng. **30**, 113 (2009).
[11] M. v. Morkovin, On the many faces of transition, in *Viscous Drag Reduction*, edited by C. S. Wells (Springer, Boston, MA, 1969), pp. 1–31.
[12] D. S. Henningson and J. Kim, On turbulent spots in plane Poiseuille flow, J. Fluid Mech. **228**, 183 (1991).
[13] A. Lundbladh and A. V. Johansson, Direct simulation of turbulent spots in plane Couette flow, J. Fluid Mech. **229**, 499 (1991).
[14] L. H. Gustavsson, Energy growth of three-dimensional disturbances in plane Poiseuille flow, J. Fluid Mech. **224**, 241 (1991).
[15] K. M. Butler and B. F. Farrell, Three-dimensional optimal perturbations in viscous shear flow, Phys. Fluids A **4**, 1637 (1992).
[16] S. C. Reddy and D. S. Henningson, Energy growth in viscous channel flows, J. Fluid Mech. **252**, 209 (1993).
[17] M. C. Sukop, *Lattice Boltzmann Modeling* (Springer, Berlin, Heidelberg, 2006).
[18] Q. Zou and X. He, On pressure and velocity boundary conditions for the lattice Boltzmann BGK model, Phys. Fluids **9**, 1591 (1997).
[19] X. He and L.-S. Luo, Lattice Boltzmann model for the incompressible Navier–Stokes equation, J. Stat. Phys. **88**, 927 (1997).
[20] U. Frisch, B. Hasslacher, and Y. Pomeau, Lattice-Gas automata for the Navier-Stokes Equation, Phys. Rev. Lett **56**, 1505 (1986).
[21] S. Chen and G. D Doolen, Lattice Boltzmann method for fluid flows, Annu. Rev. Fluid Mech. **30**, 329 (1998).
[22] S. Succi, *The Lattice-Boltzmann Equation* (Oxford University Press, Oxford, 2001).
[23] J. Bernsdorf, Th. Zeiser, G. Brenner, and F. Durst, Simulation of a 2D channel flow around a square obstacle with lattice-Boltzmann (BGK) automata, Int. J. Modern Phys. C **9**, 1129 (1998).
[24] L. Djenidi, Lattice-Boltzmann simulation of grid-generated turbulence, J. Fluid Mech. **552**, 13 (2006).
[25] J. Jeong and F. Hussain, On the identification of a vortex, J. Fluid Mech. **285**, 69 (1995).
[26] M. S. Acarlar and C. R. Smith, A study of hairpin vortices in a laminar boundary layer. Part 1. Hairpin vortices generated by a hemisphere protuberance, J. Fluid Mech. **175**, 1 (1987).
[27] P.-Å. Krogstad, H. I. Andersson, O. M. Bakken, and A. Ashrafian, An experimental and numerical study of channel flow with rough walls, J. Fluid Mech. **530**, 327 (2005).
[28] S. A. Orszag and A. T. Patera, Secondary instability of wall-bounded shear flows, J. Fluid Mech. **128**, 347 (1983).
[29] J. O. Hinze, *Turbulence* (McGraw-Hill, New York, 1975), Vol. 218.
[30] S. Tardu, Forcing a low Reynolds number channel flow to generate synthetic turbulent-like structures, Comput. Fluids **55**, 101 (2012).